Sustainable Carbon Dot-Based Fluorosensor Integrated with a Microcontroller-Driven Portable Device for On-Site Nanomolar Detection of Picric Acid

Mallika Phull[a], Amjad Ali[a], Jobanpreet Brar[b], Amit Mishra[b] and Banibrata Maity[a*]

[a]Department of Chemistry and Biochemistry, Thapar Institute of Engineering and Technology, Patiala, 147004, India. E-mail: phullmallika96@gmail.com, amjadali@thapar.edu

[b]Department of Electronics and Communication Engineering, Thapar Institute of Engineering and Technology, Patiala, 147004, India. E-mail: amit_mishra@thapar.edu

[*]*Corresponding Author E-mail: banibrata.maity@thapar.edu (Banibrata Maity)*

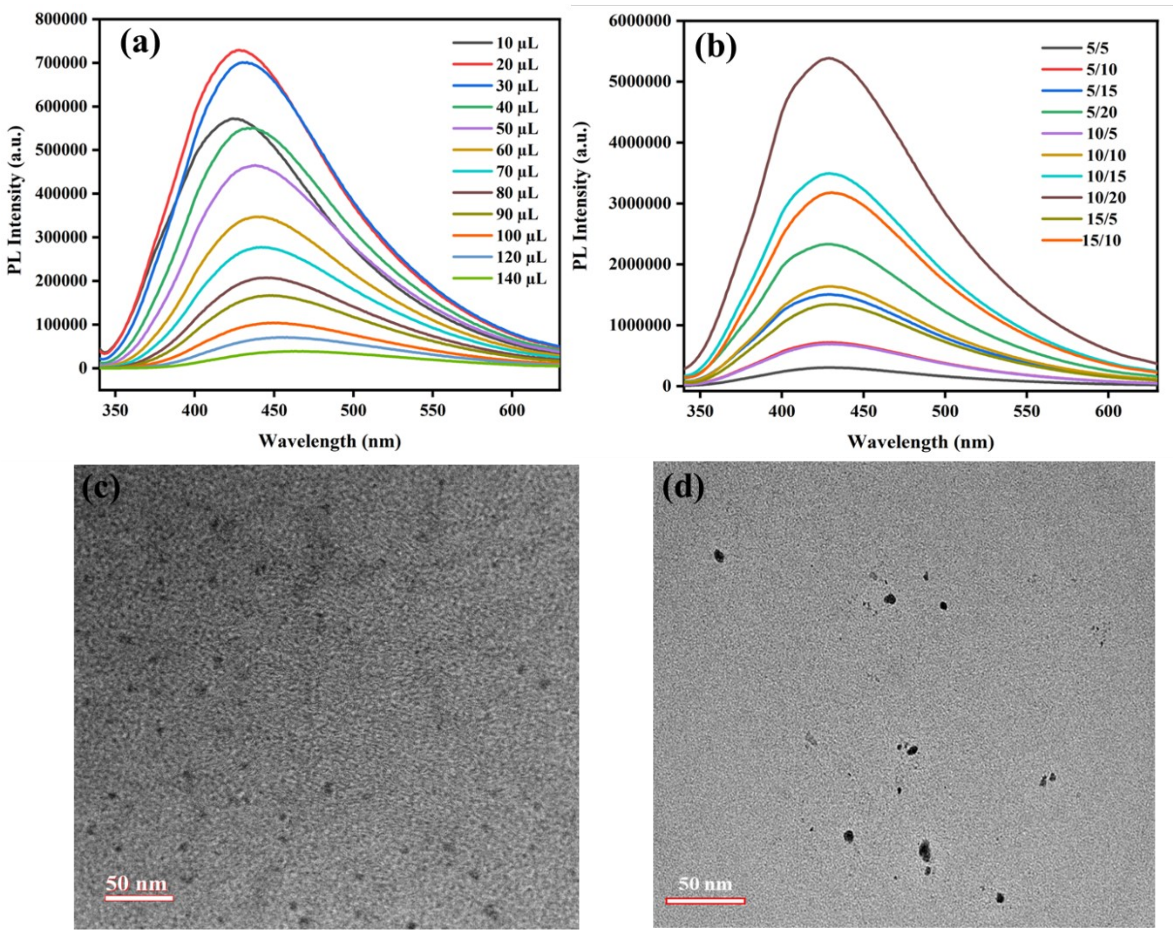

Fig. S1. (a) Volume optimization (b) Slit width optimization of W-CDs (c) and (d) HRTEM images of W-CDs at 50 nm resolution.

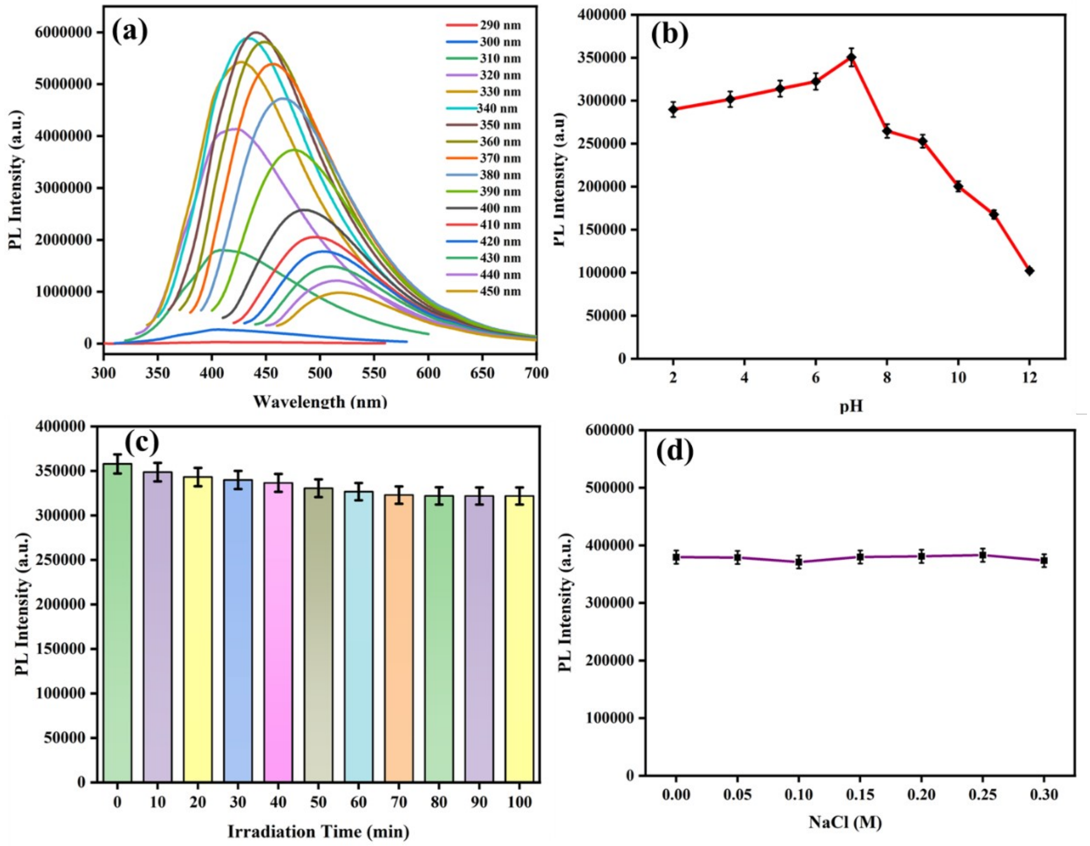

Fig. S2. (a) Excitation wavelength-dependent emission spectra (b) emission spectra at varying pH (2–12), (c) photostability assessment of W-CDs over irradiation time, and (d) effect of ionic strength on the PL intensity of W-CDs at different NaCl concentrations.

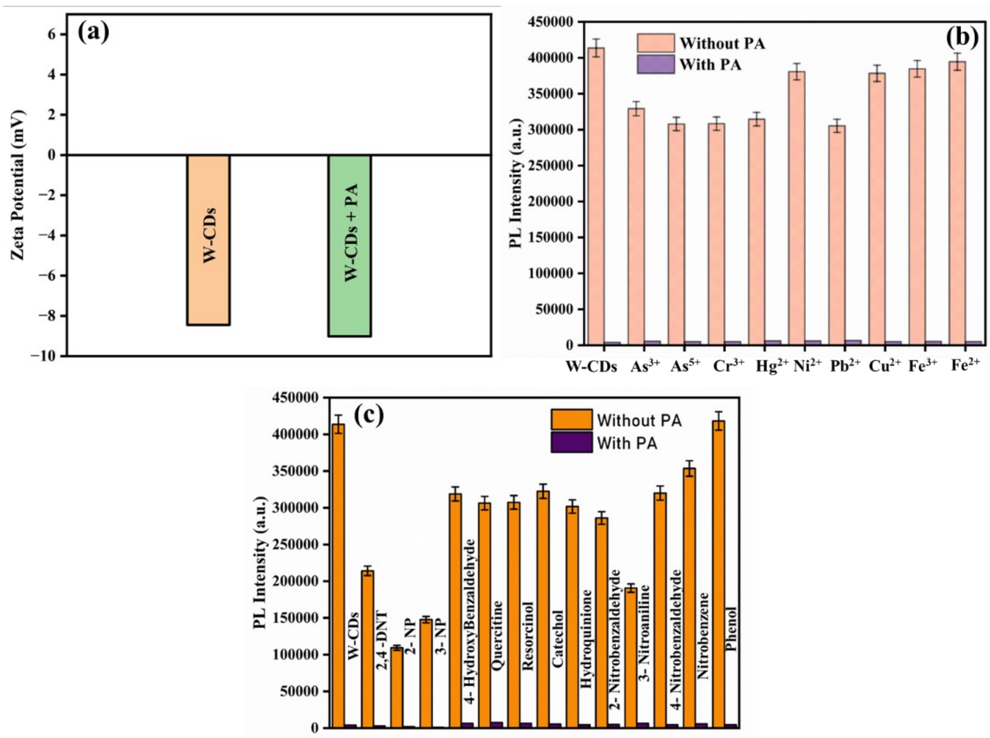

Fig. S3. (a) Zeta analysis of W-CDs and W-CDs in presence of PA, (b) Interference study of W-CDs for PA in presence of different metal ions and (c) organic analytes.

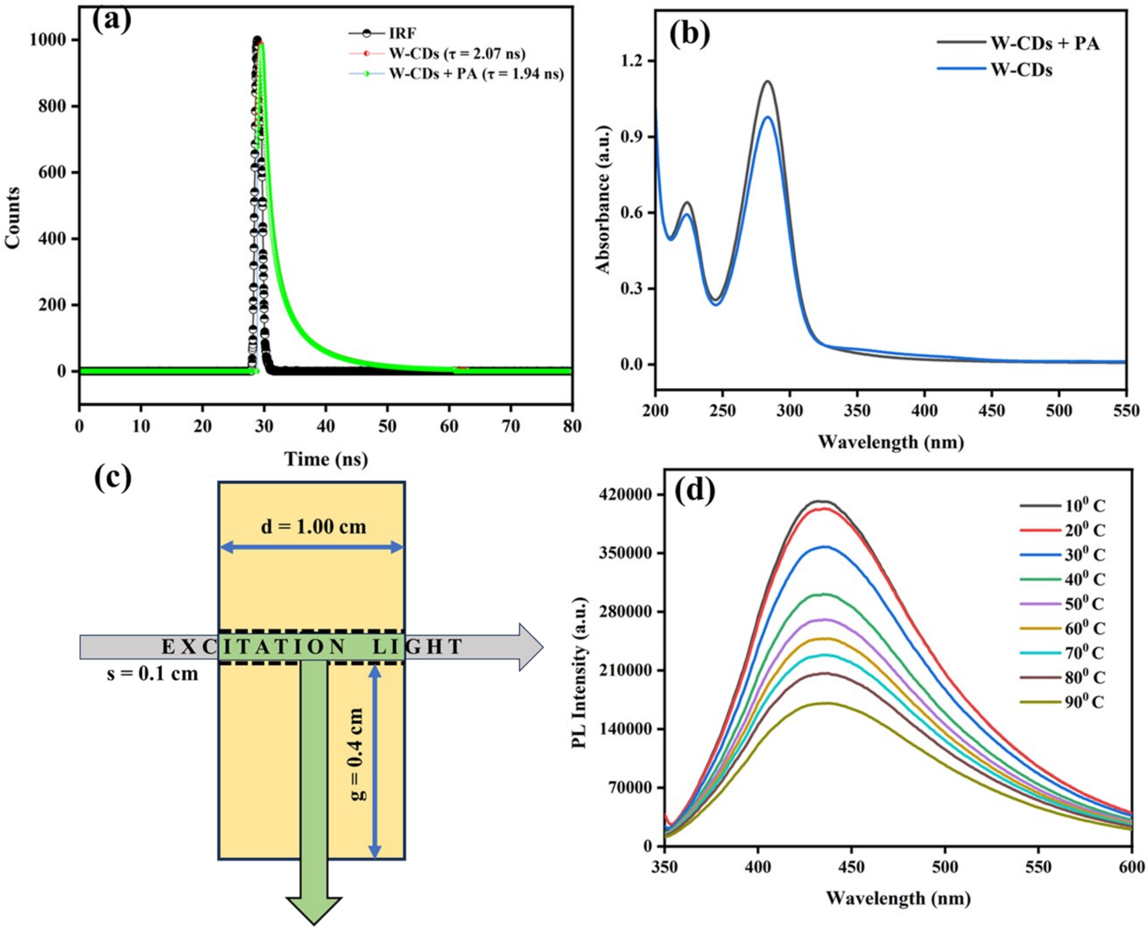

Fig. S4. (a) Fluorescence lifetime decay of W-CDs in the presence of PA, (b) UV-Vis absorption spectra of W-CDs in presence of PA, (c) effect of temperature on W-CDs and (d) schematic geometry of IFE fluorescence correction measurements.

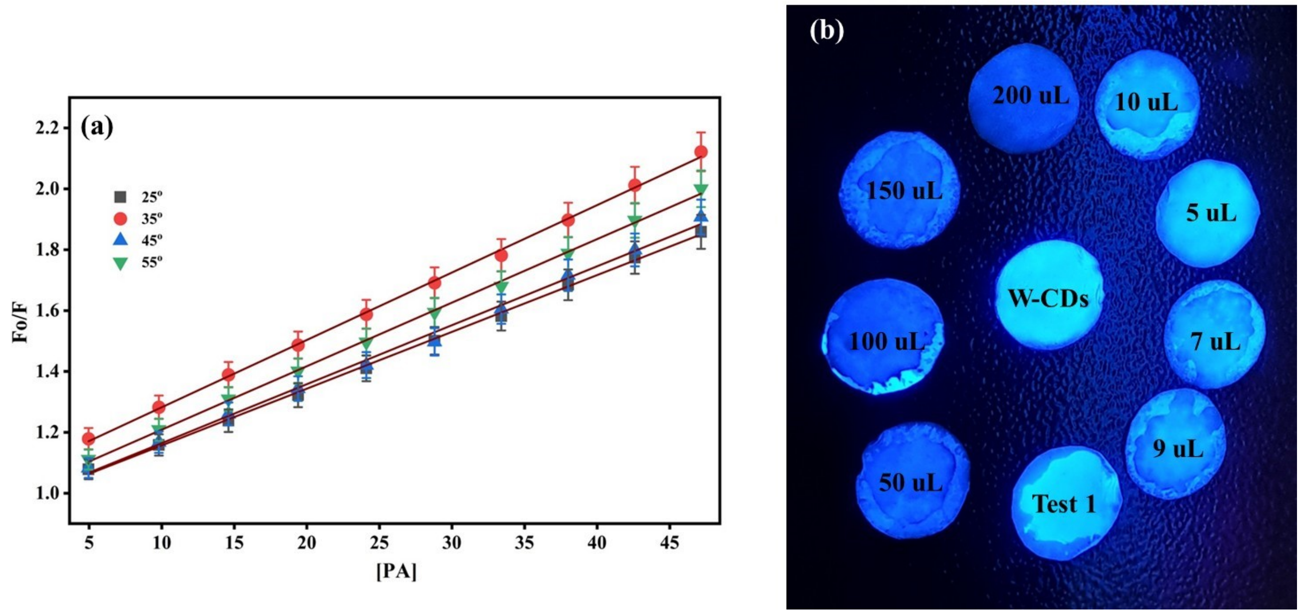

Fig. S5. (a) Temp dependent K_{S-V} determination and (b) Visual depiction of PL quenching of PA on W-CDs coated strips.

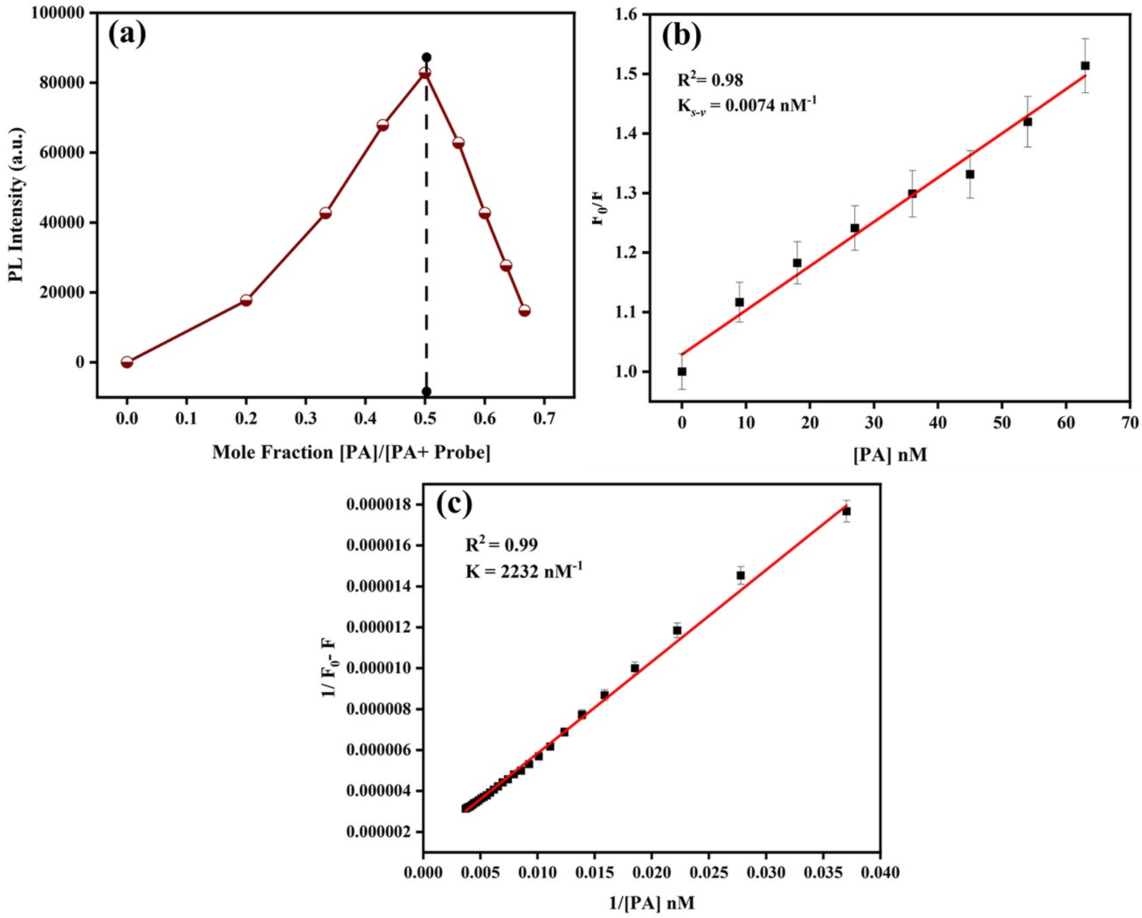

Fig. S6. (a) Job's Plot, (b) Stern-Volmer plot of W-CDs, (c) B–H plot illustrating the interaction between PA and W-CDs.

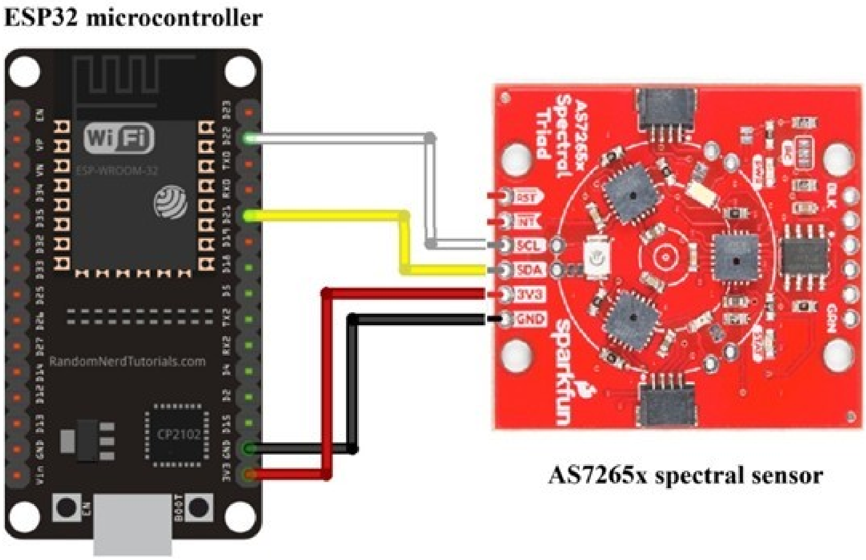

Fig. S7. Interfacing circuit between microcontroller ESP32 and spectral sensor

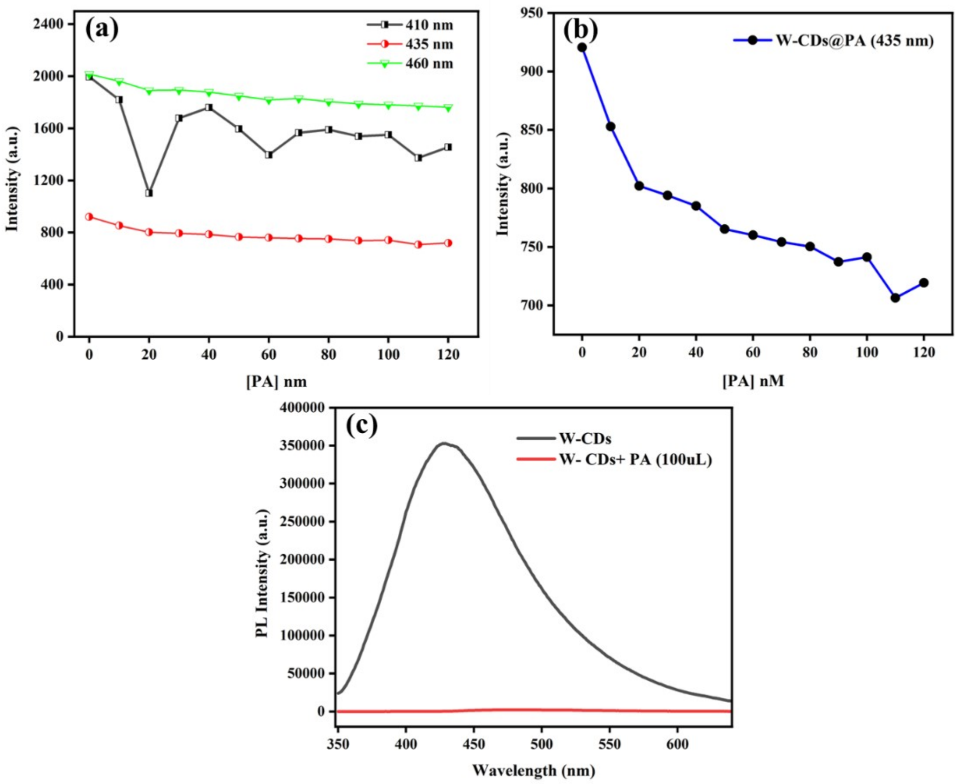

Fig. S8. (a) Normalised intensity at UV detector for three wavelengths (410 nm, 435 nm, and 460 nm) reflected from sample at different PA concentrations, (b) Intensity of different PA concentrations for wavelength 435 nm at UV detector and (c) instrument result verification by portable device data.

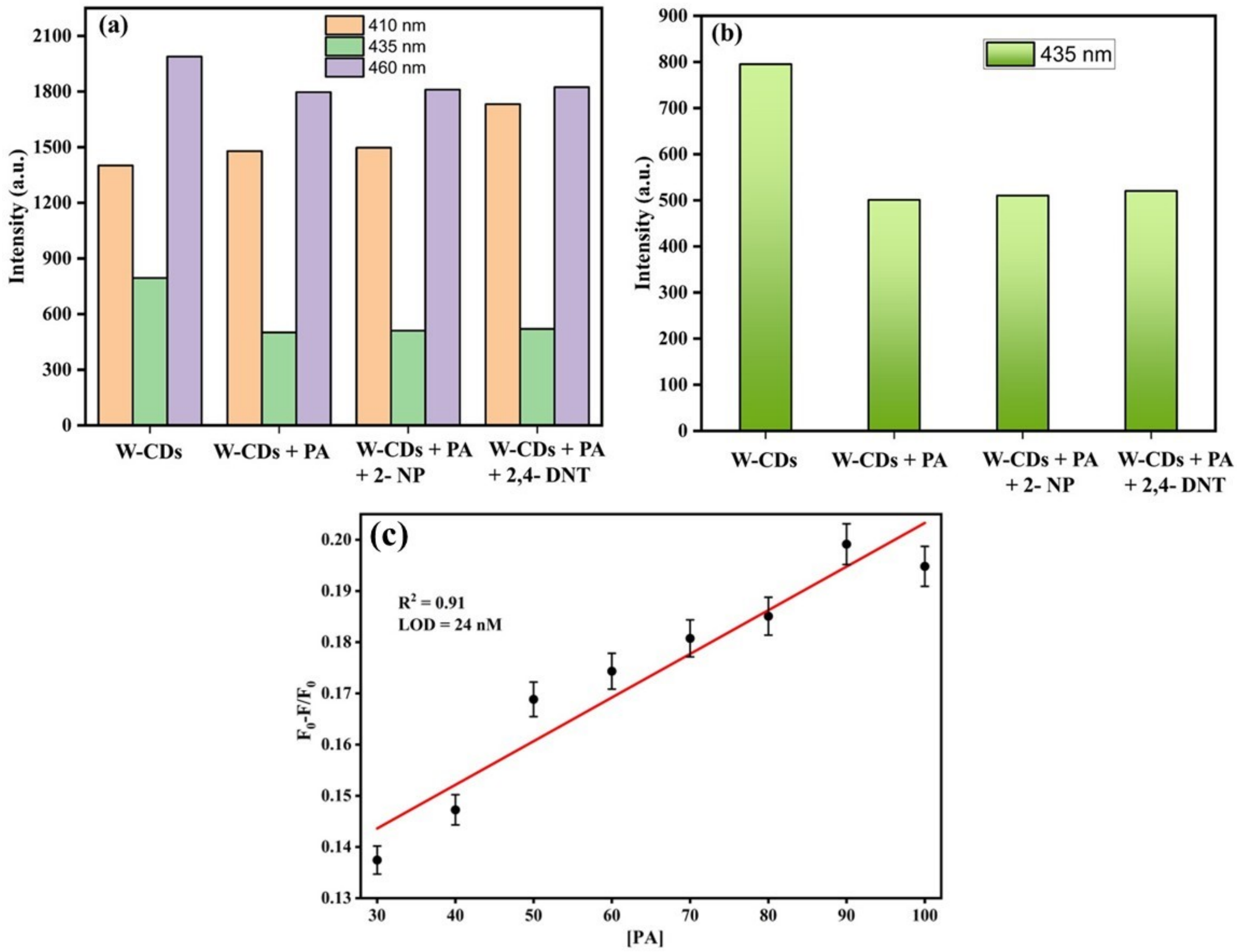

Fig. S9. Interference study (a,b) of W-CDs for PA in presence of different metal ions by portable device and (c) LOD evaluation by sensor.

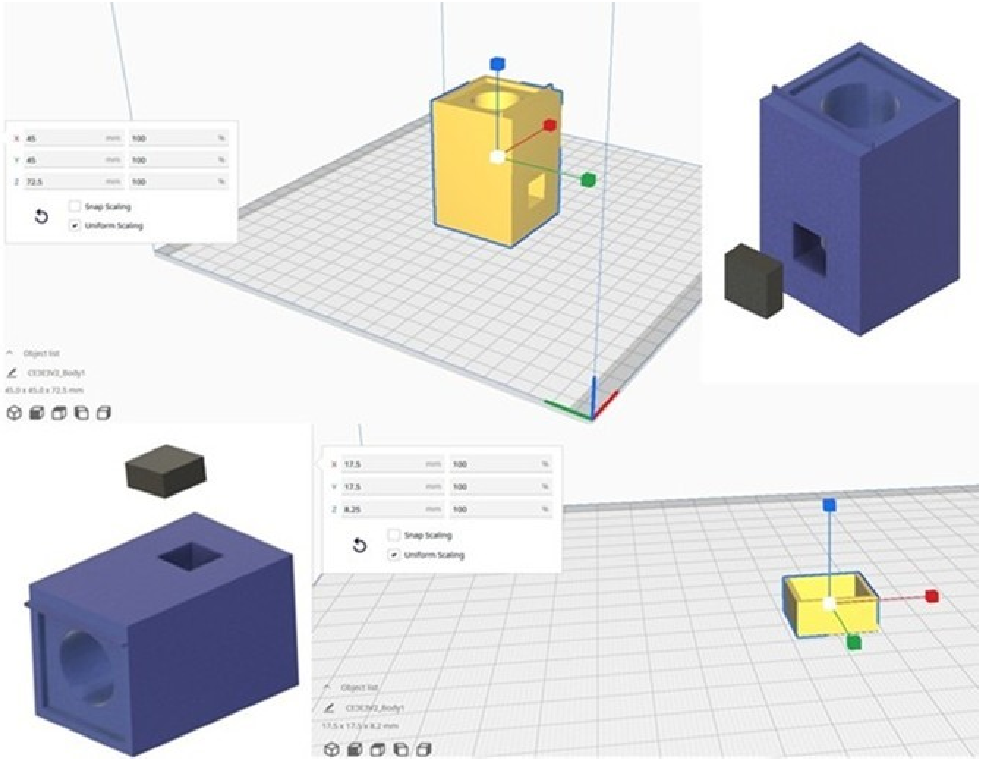

Figure S10. 3D-print design of device housing using Tinkercad.

Table S1. Photophysical parameters of W-CDs in presence of PA.

System	Φ_f**(%)**	τ_f **(ns)**	k_r**(ns^{-1})**	k_{nr}**(ns^{-1})**
W-CDs	29	2.07	0.13	0.35
W-CDs + PA	2	1.94	0.01	0.50

Error limit = ± 5%

Table S2. Temperature-dependent variation of quenching constant ($K_{S\text{-}V}$) for the W-CDs–PA system

System	Temperature (ºC)	$K_{S\text{-}V}$ (nM^{-1})	R^2
W-CDs + PA	25	0.019	0.99
	35	0.022	0.99
	45	0.019	0.99
	55	0.020	0.99

Table S3. Intraday and interday precision data for PA estimation using the developed W-CDs sensor.

Analyte	Conc. (nM)	Intraday[a]		Interday[b]	
		%RSD	%Error[c]	%RSD	%Error[c]
PA	66	1.30	0.75	0.62	0.36
	132	1.35	0.78	0.23	0.13
	198	1.31	0.76	0.30	0.17

Each result is the average of three separate determinations.

[a]Within a day

[b]Three consecutive days

[c]%Error = %RSD/$\sqrt{n}$

Table S4. UV detector data at three wavelengths (410 nm, 435 nm, and 460 nm) for PA in portable device.

Concentration (nM)	410 nm	435 nm	460 nm
0	1995.9	920.59	2015.1
10	1819.38	852.84	1962.67
20	1102.45	802.12	1891.18
30	1677.82	794.06	1894.04
40	1759.43	785.02	1878.79
50	1596.22	765.16	1849.24
60	1395.55	760.1	1818.73
70	1566.25	754.2	1829.22
80	1589.56	750.22	1804.44
90	1538.77	737.27	1788.23
100	1549.59	741.25	1781.56
110	1373.9	706.38	1772.03
120	1455.5	719.33	1762.49

Table S5. Interference study by portable device.

Concentration (nM)	410 nm	435 nm	460 nm
W-CDs (Blank)	1401.38	795.05	1988.41
Blank + 100uL PA	1478.82	500.87	1796.31
Blank + 100uL PA + 300uL 2NP	1497.14	510.29	1810.16
Blank + 100uL PA + 300uL 2,4 DNT	1731.95	520.13	1823.5

Scheme 1. Video depicting qualitative detection of PA in test sample by portable device.

IMG_6244.mp4

4.3. Methodology

The experimental apparatus utilized in this study was developed as a prototype for a portable system, prioritizing reproducibility and ease of manufacturing, to enable rapid evaluation of a sample's internal features under field settings. There are mainly three modalities to evaluate nitroaromatic, PA, such as transmittance, reflectance, and interactance. In this experiment, interactance mode is used to evaluate the spectral characteristics of the sample through the proposed sensor based embedded system. In this system both UV light source and detector are mounted on a single PCB and placed opposite to a reflector surface.[1] The spectral measurements are conducted by positioning a sample-filled cuvette in front of the light source and sensor combination. This mode is especially well-suited for portable devices. Based on spectral qualities, interactance is thought to be the most efficient way to infer internal characteristics of samples.[2]

1. Nicolai, B. M.; Beullens, K.; Bobelyn, E.; Peirs, A.; Saeys, W.; Theron, K. I.; Lammertyn, J. Nondestructive Measurement of Fruit and Vegetable Quality by Means of NIR Spectroscopy: A Review. *Postharvest Biol. Technol.* **2007**, *46* (2), 99–118. https://doi.org/10.1016/j.postharvbio.2007.06.024

2. Schaare, P. N.; Fraser, D. G. Comparison of Reflectance, Interactance and Transmission Modes of Visible-Near Infrared Spectroscopy for Measuring Internal Properties of Kiwifruit

(*Actinidia chinensis*). *Postharvest Biol. Technol.* **2000**, *20* (2), 175–184. https://doi.org/10.1016/S0925-5214(00)00126-8